

SuperFlow: Training Flow Matching Models with RL on the Fly

Kaijie Chen^ε, Zhiyang Xu^θ, Ying Shen^η, Zihao Lin^ς, Yuguang Yao^ν, Lifu Huang^ς✉

Abstract

Recent progress in flow-based generative models and reinforcement learning (RL) has significantly improved text–image alignment and visual quality. However, existing RL training methods for flow models still suffer from two critical limitations: (i) GRPO-style *fixed* per-prompt group sizes ignore heterogeneous sampling importance across prompts, leading to inefficient computation allocation and slower convergence; and (ii) trajectory-level advantages are commonly reused as per-step estimates, which introduces biased credit assignment along continuous-time flow trajectories. We propose **SuperFlow**, a novel RL training framework for flow-based models that addresses both issues. Specifically, **SuperFlow** introduces a variance-aware sampling strategy that dynamically adjusts group sizes according to prompt-level uncertainty, and derives step-level advantage estimates that are grounded in continuous-time flow dynamics. Empirically, **SuperFlow** achieves state-of-the-art performance among RL-optimized flow-based text-to-image models, while requiring only 5.4% ~ 56.3% of the original training steps and reducing wall-clock training time by 5.2% ~ 16.7%, without any architectural modifications. Across standard text-to-image benchmarks, including text rendering, compositional generation, and human preference alignment, **SuperFlow** improves over SD3.5-M by 4.6% ~ 47.2% and over FLOW-GRPO by 1.7% ~ 16.0%.

1 Introduction

Modern text-to-image (T2I) generation systems are typically trained in two stages: large-scale pretraining on web-scale data, followed by post-training for task-specific objectives (e.g., high-resolution

fidelity, compositional correctness, or text rendering) (Podell et al., 2023a; Saharia et al., 2022; Esser et al., 2024a; Labs et al., 2025; Fan et al., 2025; Chen et al., 2025a). Recently, online reinforcement learning (RL) has emerged as a promising post-training mechanism for further enhancing their ability to compose complex scenes and accurately render text (He et al., 2025; Luo et al., 2025a; Ding and Ye, 2025; Tian et al., 2025; Luo et al., 2025b; Chen et al., 2025b). Among them, Flow-GRPO (Liu et al., 2025) reformulates the deterministic Ordinary Differential Equation (ODE) used in flow-matching into an equivalent Stochastic Differential Equation (SDE), thereby enabling RL-based exploration during the sampling process. While this method demonstrates substantial performance gains, it still faces several critical challenges.

(1) **Sampling Inefficiency.** Flow-GRPO typically relies on a fixed number of group samples (e.g., up to 64) per prompt, leading to substantial computational overhead and inefficient use of sampling budgets (Xu and Ding, 2025). In practice, prompts differ significantly in reward variance and learning potential: some exhibit highly informative reward signals, while others yield nearly constant reward returns (Le et al., 2025). From the GRPO objective (Shao et al., 2024), the expected gradient magnitude scales with the variance of returns, implying that high-variance prompts contribute disproportionately to policy improvement (Sutton et al., 1999). Uniform sampling, therefore, wastes computation on low-variance prompts while under-sampling informative ones, motivating adaptive and variance-aware sampling strategies.

(2) **Training Instability.** As training progresses, policy outputs tend to become increasingly homogeneous, leading to low reward variance within sampling groups. In such cases, relative advantages collapse toward zero, weakening gradient signals and accelerating entropy collapse (Cui et al., 2025). This instability is particularly severe in later train-

^ε Tongji University ^θ Virginia Tech ^η University of Illinois Urbana-Champaign ^ς University of California, Davis ^ν Intuit. Primary Contact: <2252538@tongji.edu.cn>

ing stages and calls for optimization mechanisms that remain informative even when reward variance is limited.

(3) **Inaccurate Step-Level Advantage Estimation.** Current reinforcement learning pipelines for flow-based generative models suffer from inaccurate advantage estimation (Ding and Ye, 2025; He et al., 2025). In GRPO, trajectory-level advantages are computed via normalization of rewards within each sampling group, implicitly assuming sufficient reward variance and reliable relative ranking among samples. While DeepSeekMath (Shao et al., 2024) partially alleviates this issue by incorporating process-level rewards in GRPO for language generation, such signals are substantially more difficult to obtain in flow-based image generation, as the intermediate states along the denoising trajectory are usually visually noisy and semantically ambiguous (Zhang et al., 2025a). Recent approaches attempt to approximate the contribution of intermediate states using heuristics such as cosine similarity between latent representations (Zhang et al., 2025b). However, these methods yield only marginal performance gains and fail to fundamentally address the bias inherent in group-normalized advantage estimation, leaving advantage signals unreliable and limiting the effectiveness of RL-based optimization.

To address these three fundamental challenges, we propose **SuperFlow**, a novel reinforcement learning algorithm that improves training efficiency and stability while enabling effective estimation of process-level rewards for flow-matching models. To mitigate the inefficiency and instability caused by uniform sampling, we introduce **Dynamic-Group Sampling**, which adaptively adjusts the number of samples based on *reward uncertainty*: prompts with higher reward uncertainty indicate greater learning potential and are therefore prioritized and allocated more rollouts.

By focusing computation on the most informative prompts, both designs substantially improve sampling efficiency and stabilize training dynamics. Moreover, using a running-average reward baseline instead of per-group normalization reduces variance in advantage estimates and mitigates entropy collapse in later training stages.

In addition, we propose **Step-level Advantage Re-estimation** to address bias arising from trajectory-level advantage estimation in flow-based training. Existing methods reuse a single trajectory-level advantage across all denoising steps, despite

the fact that reward distributions and uncertainty vary substantially over the denoising process. To resolve this issue, we re-estimate advantages at each denoising step using step-dependent statistics, including the reward standard deviation. This yields more accurate and consistent credit assignment to intermediate states, leading to improved training stability and stronger alignment with reward objectives.

Extensive experiments demonstrate that **SuperFlow** achieves comparable or superior performance to prior reinforcement learning methods while requiring fewer training steps and substantially reduced computational cost. We evaluate **SuperFlow** on multiple text-to-image tasks with diverse reward formulations. On standard benchmarks, **SuperFlow** improves GenEval by 38.4% over SD3.5-M and by 2.8% over FLOW-GRPO, improves OCR accuracy by 47.2% and 16.0% over the same baselines, respectively, and achieves gains of 4.6% and 1.7% on PickScore. These results indicate that **SuperFlow** generalizes effectively across different reward types and maintains stable performance under varied training objectives.

To summarize, the contributions of **SuperFlow** are as follows:

- We propose **SuperFlow**, a reinforcement learning framework for flow-matching text-to-image models that improves training efficiency and stability across diverse reward settings.
- We introduce two key components: (1) dynamic-group sampling, which allocates samples per prompt based on reward uncertainty to improve efficiency and stability, and (2) step-level advantage re-estimation, which enables more accurate credit assignment along the denoising trajectory.
- Extensive experiments on multiple text-to-image benchmarks show that **SuperFlow** matches or outperforms prior RL methods while requiring fewer training steps and lower computational cost.

2 Related Work

Reinforcement Learning for Large Language Models. Reinforcement learning has been widely used to post-train large language models under preference-based or verifiable rewards. Proximal Policy Optimization (PPO) (Schulman et al., 2017)

and its variants are effective for RLHF-style training, but often require a learned critic and careful tuning to maintain stability. Group Relative Policy Optimization (GRPO) (Shao et al., 2024) offers a critic-free alternative by using multiple samples per prompt to form a group-relative baseline and normalize rewards into advantages, and has shown strong performance in instruction following and reasoning (Liu et al., 2024).

More recently, Single-Stream Policy Optimization (SPO) (Xu and Ding, 2025) performs single-sample updates and relies on streaming statistics or tracking mechanisms to stabilize advantage estimation and normalization over time. These methods offer an important path to reduce the generation overhead of group-based methods while still enabling effective reward-driven learning for generative models.

Reinforcement Learning for Diffusion and Flow Matching. Reinforcement learning has also been a powerful tool for steering diffusion and flow-based text-to-image models toward task- or preference-aligned objectives.

Some approaches integrate RL signals directly into model training. For example, Q-score Matching (QSM) (Psenka et al., 2023) optimizes generative models against explicit reward signals, using vision-language models as outcome reward models, while DPOK (Fan et al., 2023) introduces an online RL framework for diffusion models. These ideas have been instantiated in diffusion+DPO (Wallace et al., 2024; Chen et al., 2025c) and diffusion+PPO (Ren et al., 2024), demonstrating that moving beyond pure likelihood training can improve image fidelity and semantic alignment. Motivated by the success of GRPO in LLMs, several works adapt GRPO-style updates to the structure of diffusion and flow matching. Flow-GRPO (Liu et al., 2025) converts the deterministic ODE to an equivalent SDE, preserving marginals while enabling reliable sampling for RL. Dance-GRPO (Xue et al., 2025), Mix-GRPO (Li et al., 2025), and Temp-GRPO (He et al., 2025) further tailor GRPO updates to different aspects of the denoising process.

Although GRPO-based methods for diffusion and flow matching report consistent improvements over purely supervised baselines, they inherit limitations from the underlying group-based formulation. Fixed-size per-prompt groups lead to inefficient and inflexible sampling allocation, and

on-the-fly per-group baselines increase generation cost and synchronization overhead in distributed settings. In addition, trajectory-level advantages obtained via simple group-wise normalization can be biased for continuous-time flows, where intermediate states are noisy and difficult to credit accurately, even when augmented with heuristic step-level rewards (Liao et al., 2025; Zhang et al., 2025b). Our work addresses these challenges for flow matching by introducing a Streaming-to-Group sampling scheme that adaptively allocates samples across prompts while retaining the benefits of group-wise normalization, and a step-level advantage re-estimation mechanism that provides more accurate credit assignment along the denoising trajectory.

3 Preliminaries

In this section, we introduce the mathematical formulation of flow matching and explain how GRPO is applied to flow matching models.

Flow Matching. Let $\mathbf{x}_0 \sim X_0$ be a data sample from the target data distribution, and let $\mathbf{x}_1 \sim X_1$ denote a noise sample. We adopt the Rectified Flow framework (Liu et al., 2023), which defines the noised sample at continuous time $\tau \in [0, 1]$ as

$$\mathbf{x}_\tau = (1 - \tau) \mathbf{x}_0 + \tau \mathbf{x}_1, \quad (1)$$

A denoising model is trained to predict the velocity field $\mathbf{v}_\theta(\mathbf{x}_\tau, \tau)$ by minimizing the flow matching objective (Lipman et al., 2022; Liu et al., 2023):

$$\mathcal{L}(\theta) = \mathbb{E}_{\tau, \mathbf{x}_0 \sim X_0, \mathbf{x}_1 \sim X_1} [\|\mathbf{v} - \mathbf{v}_\theta(\mathbf{x}_\tau, \tau)\|^2], \quad (2)$$

where the target velocity field is $\mathbf{v} = \mathbf{x}_1 - \mathbf{x}_0$.

Denoising as an MDP. Following Black et al. (2023), the reverse-time denoising procedure of the rectified flow can be formalized as a Markov Decision Process (MDP) $(\mathcal{S}, \mathcal{A}, \rho_0, P, R)$. We denote the state at denoising step t as $\mathbf{s}_t \triangleq (\mathbf{c}, t, \mathbf{x}_t)$, where \mathbf{c} represents the conditioning prompt. The action is the next denoised sample $\mathbf{a}_t \triangleq \mathbf{x}_{t-1}$, and the policy is

$$\pi_\theta(\mathbf{a}_t | \mathbf{s}_t) \triangleq p_\theta(\mathbf{x}_{t-1} | \mathbf{x}_t, \mathbf{c}), \quad (3)$$

The transition is deterministic:

$$P(\mathbf{s}_{t+1} | \mathbf{s}_t, \mathbf{a}_t) \triangleq (\delta_{\mathbf{c}}, \delta_{t-1}, \delta_{\mathbf{x}_{t-1}}), \quad (4)$$

and the initial state distribution is $\rho_0(\mathbf{s}_0) \triangleq (p(\mathbf{c}), \delta_T, \mathcal{N}(\mathbf{0}, \mathbf{I}))$, where δ_x is the Dirac delta distribution centered at x .

The reward is given only at the final step:

$$R(\mathbf{s}_t, \mathbf{a}_t) \triangleq \begin{cases} r(\mathbf{x}_0, \mathbf{c}), & t = 0 \\ 0, & \text{otherwise} \end{cases} \quad (5)$$

Formulation of Sampling SDEs. Since GRPO (Shao et al., 2024) requires stochastic exploration through multiple trajectory samples, Liu et al. (2025) further constructs a reverse-time SDE formulation for the flow-based models to enable stochastic sampling:

$$d\mathbf{x}_t = \left[\mathbf{v}_t(\mathbf{x}_t) + \frac{\sigma_t^2}{2t}(\mathbf{x}_t + (1-t)\mathbf{v}_t(\mathbf{x}_t)) \right] dt + \beta_t d\mathbf{w}, \quad (6)$$

where $d\mathbf{w}$ denotes Wiener process increments and σ_t control the level of stochasticity during generation.

4 Revisiting SPO for Flow Matching

4.1 Single-Stream Policy Optimization

Recently, Single-Stream Policy Optimization (SPO) (Xu and Ding, 2025) introduces a framework that enables online policy updates using streaming rollouts by maintaining a per-prompt tracker to stabilize advantage normalization without sampling multiple rollouts.

Specifically, for each prompt c in the training set \mathcal{C} , SPO maintains a value tracker $\hat{v}(c)$ that stores the running estimate of the expected reward for prompt c . Specifically, $\hat{v}(c)$ is modeled using a Beta distribution $\hat{v}(c) \sim \text{Beta}(\alpha(c), \beta(c))$.

During policy learning, SPO (Xu and Ding, 2025) updates the prompt-level value tracker $\hat{v}(c)$ upon observing a new reward $r(c, y)$ for prompt c and generated response y :

$$\alpha(c) = \rho(c) \alpha_{-1}(c) + r(c, y), \quad (7)$$

$$\beta(c) = \rho(c) \beta_{-1}(c) + (1 - r(c, y)), \quad (8)$$

$$\hat{v}(c) = \frac{\alpha(c)}{\alpha(c) + \beta(c)}, \quad (9)$$

where $(\alpha_{-1}, \beta_{-1})$ denote the prior Beta parameters from the previous update. The discount factor $\rho(c) = 2^{-D(c)/D_{\text{half}}}$ controls how fast the tracker forgets old data. More details on the initialization and its hyperparameters can be found in Appendix B. SPO uses the tracker’s estimate \hat{v} as a baseline for advantage calculation to support single-stream policy optimization. At each iteration, the advantage can be computed using the

pre-update baseline and the reward from a single rollout: $A(c, y) = r(c, y) - \hat{v}_{i-1}(c)$, where $\hat{v}_{i-1}(c)$ is the pre-update baseline at training iteration $i - 1$.

SPO prioritizes prompts with the highest learning potential by defining an uncertainty score based on the tracker $\hat{v}_{i-1}(c)$ for each prompt c at iteration i :

$$w_i(c) \propto \sqrt{\hat{v}_{i-1}(c)(1 - \hat{v}_{i-1}(c))} + \epsilon, \quad (10)$$

where ϵ is a small constant that ensures every prompt has a nonzero sampling probability. Higher weights denote greater reward uncertainty, thereby increasing the visitation frequency of prompts with high learning potential.

4.2 Limitations of SPO in Flow Matching

While Single-Stream Policy Optimization (SPO) (Xu and Ding, 2025) with single-rollout has demonstrated strong performance in large language model reasoning tasks, directly applying SPO to flow matching presents fundamental challenges.

To study this setting, we apply SPO directly to flow-matching models for text-to-image generation under multiple reward formulations. As shown in Figure 1, SPO exhibits unstable training behavior in later stages: although performance initially improves, it degrades sharply after prolonged training and eventually collapses. As the training progresses, sampled rewards are often close to the running baseline estimate for some prompts, leading to near-zero normalized advantages and weak gradient signals under the loss function. In such cases, learning progress can slow or stall. Consequently, this suggests that naively applying SPO to flow matching is insufficient, motivating the need for designing better mechanisms to achieve efficient and stable optimization in flow-based generative models.

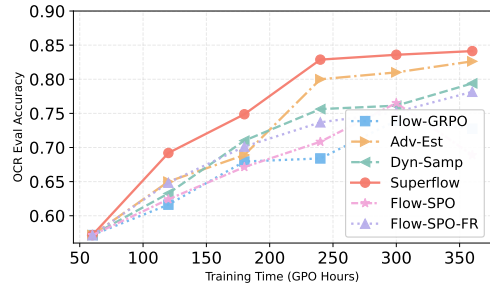


Figure 1: Training dynamics of different models on the OCR task.

5 Methodology

We introduce SuperFlow, an efficient and stable framework for policy optimization in flow match-

ing models. SuperFlow consists of two key components: **Dynamic-Group Sampling**, a variance-aware sampling strategy that adaptively adjusts group sizes based on prompt-level uncertainty, and **Step-level Advantage Re-estimation**, which computes step-wise advantage estimates grounded in the underlying continuous-time flow dynamics. Together, these components enhance training stability and sample efficiency, while yielding improved generative quality in flow-based models.

5.1 Dynamic-Group Sampling

We first propose **Dynamic-Group Sampling** that adaptively adjust the number of sampling rollouts per prompts only when necessary, balancing the efficiency of streaming updates with the stability of group-based normalization.

For each training iterations, we compute a prompt-level uncertainty score $w(c)$ using Eq. 10 for all prompts. We then partition the scores $w(c)$ into K uniform bins with thresholds $\{q_k\}_{k=0}^K$. We assign each prompt a bin index:

$$b(c) = k \quad \text{s.t.} \quad s(c) \in [q_{k-1}, q_k). \quad (11)$$

The bin index $b(c)$ is further mapped to a per-prompt rollout count $m(c)$ via a linear rule:

$$m(c) = M_{\max} - b(c) + 1, \quad (12)$$

where we choose $M_{\max} \geq K$, to ensure that every prompt receives at least one rollout. Thus, prompts with lower reward uncertainty receive more rollouts to stabilize group normalization, while prompts with higher reward uncertainty receive fewer rollouts to save computation.

5.2 Step-level Advantage Re-estimation

Standard FLOW-GRPO (Liu et al., 2025) training typically computes a single trajectory-level advantage and reuses it as the step-level advantage for all denoising steps. However, this uniform assignment could lead to biased credit assignment, as it fails to account for the variation in significant reward uncertainty and action variability along the denoising trajectory. To address this, we propose a lightweight **step-level advantage re-estimation** mechanism that modulates the trajectory-level advantage to match step-dependent statistics.

We start with the standard Monte Carlo advantage formulation with a baseline b :

$$A_t = \sum_{s=t}^T \gamma^{s-t} r(y_s) - b, \quad (13)$$

where $\gamma \in [0, 1]$ is a discount factor and $r(y_s)$ is the reward at step s .

Evaluating rewards at every intermediate denoising step is often computationally prohibitive. To approximate step-wise advantages efficiently, we redistribute the trajectory-level signal based on step-dependent uncertainty. We define the re-estimated step-level advantage \hat{A}_t as:

$$\hat{A}_t = w_t \cdot A^\tau, \quad w_t = \eta \sigma_t, \quad (14)$$

where A^τ is the trajectory-level advantage derived from the final reward, and σ_t is the standard deviation of the conditional action distribution $p_\theta(\mathbf{x}_{t-1} | \mathbf{x}_t, \mathbf{c})$ at step t , and η is a hyperparameter that controls how strongly σ_t is modulated across steps. In the flow-matching setting, σ_t is essentially the diffusion coefficient of the reverse-time SDE at time t in Eq. 6.

6 Experiments

This section presents an empirical evaluation of SuperFlow under three representative evaluation settings for flow matching models.

6.1 Experiment Setup

Datasets and Benchmarks To thoroughly evaluate the effectiveness of SuperFlow, following FLOWGRPO (Liu et al., 2025), we adopt three benchmarks spanning three domains: (1) **Visual text rendering**, which includes 20K training prompts and 1K test prompts from Liu et al. (2025), evaluated using OCRScore; (2) **Compositional image generation**, namely GenEval (Ghosh et al., 2023); (3) **Human preference alignment**, using the dataset from Liu et al. (2025) and evaluated with PickScore. Further details of these benchmarks are provided in Appendix C.2.

Implementation Details We post-train all models on a single NVIDIA H200 GPU with 141 GB of memory. Unless stated otherwise, all methods use the same backbone model, prompt pool, reward computation, and training budget to ensure a controlled comparison. Unless specified otherwise, all hyperparameters follow the default values used in Liu et al. (2025) and all hyperparameters of SuperFlow are kept fixed across tasks except for the KL ratio β . or Dynamic-Group Sampling, we set the maximum rollout count M_{max} to be 24, matching the group size configuration used in Flow-GRPO and SPO-FR, and we set the number of uniform bins K to be 4 in all experiments. We

| Model | Overall | Single Obj. | Two Obj. | Counting | Colors | Position | Attr. Binding |
|------------------------------|------------------------------|------------------------------|------------------------------|------------------------------|------------------------------|------------------------------|------------------------------|
| <i>Diffusion Models</i> | | | | | | | |
| LDM | 0.37 | 0.92 | 0.29 | 0.23 | 0.70 | 0.02 | 0.05 |
| SD1.5 | 0.43 | 0.97 | 0.38 | 0.35 | 0.76 | 0.04 | 0.06 |
| SD2.1 | 0.50 | 0.98 | 0.51 | 0.44 | 0.85 | 0.07 | 0.17 |
| SD-XL | 0.55 | 0.98 | 0.74 | 0.39 | 0.85 | 0.15 | 0.23 |
| DALLE-2 | 0.52 | 0.94 | 0.66 | 0.49 | 0.77 | 0.10 | 0.19 |
| DALLE-3 | 0.67 | 0.96 | 0.87 | 0.47 | 0.83 | 0.43 | 0.45 |
| <i>Autoregressive Models</i> | | | | | | | |
| Show-o | 0.53 | 0.95 | 0.52 | 0.49 | 0.82 | 0.11 | 0.28 |
| Emu3-Gen | 0.54 | 0.98 | 0.71 | 0.34 | 0.81 | 0.17 | 0.21 |
| JanusFlow | 0.63 | 0.97 | 0.59 | 0.45 | 0.83 | 0.53 | 0.42 |
| <i>Flow Matching Models</i> | | | | | | | |
| SD3.5-M | 0.58 ^{†0.00} | 0.98 ^{†0.00} | 0.78 ^{†0.00} | 0.50 ^{†0.00} | 0.81 ^{†0.00} | 0.24 ^{†0.00} | 0.52 ^{†0.00} |
| Flow-GRPO | 0.78 ^{†0.20} | 0.99 ^{†0.01} | 0.85 ^{†0.07} | 0.69 ^{†0.19} | 0.85 ^{†0.04} | 0.31 ^{†0.07} | 0.66 ^{†0.14} |
| Flow-SPO | 0.75 ^{†0.17} | 0.99 ^{†0.01} | 0.84 ^{†0.06} | 0.66 ^{†0.16} | 0.84 ^{†0.03} | 0.30 ^{†0.06} | 0.64 ^{†0.12} |
| SuperFlow | 0.80 ^{†0.22} | 0.99 ^{†0.01} | 0.87 ^{†0.09} | 0.72 ^{†0.22} | 0.87 ^{†0.06} | 0.33 ^{†0.09} | 0.69 ^{†0.17} |

Table 1: GenEval Results. Obj.: Object; Attr.: Attribution. We highlight the **best**.

use $T = 10$ discretization steps for flow-based sampling during RL training, and $T = 40$ steps for evaluation. Additional details can be found in the Appendix C.1.

Baselines We select six representative diffusion model baselines, including LDM (Rombach et al., 2022), SD1.5 (Rombach et al., 2022), SD2.1 (Rombach et al., 2022), SD-XL (Podell et al., 2023b), DALLE-2 (Ramesh et al., 2022), and DALLE-3 (Betker et al., 2023). We choose three autoregressive model baselines, including Show-o (Xie et al., 2024), Emu3-Gen (Wang et al., 2024), JanusFlow (Ma et al., 2024). We compare **SuperFlow** with the following baselines: (1) SD3.5-M (Esser et al., 2024b); (2) Flow-GRPO (Liu et al., 2025), which applies GRPO (DeepSeek-AI et al., 2025) to SD3.5-M; (3) Flow-SPO, which applies SPO (Xu and Ding, 2025) to SD3.5-M.

6.2 Main Results

Compositional Image Generation (GenEval). As shown in Table 1, **SuperFlow** attains an overall score of 0.8045, a relative gain of 38.4% over SD3.5-M (0.5814) and 2.8% over Flow-GRPO (0.7829) at the same number of training steps. Figure 2 and Figure 5, 6 in Appendix present the qualitative results of **SuperFlow** and baselines, across all three benchmarks. For example, in compositional image generation, for the prompt “a photo of a backpack below a cake,” SD3.5-M fails the relation (0.00), while **SuperFlow** passes exactly (1.00) by placing the backpack below the cake.

| Model | OCR Score | PickScore |
|------------------|------------------------------------|------------------------------------|
| SD3.5-M | 0.57165 ^{†0.00000} | 0.83039 ^{†0.00000} |
| Flow-GRPO | 0.72516 ^{†0.15351} | 0.85364 ^{†0.02325} |
| Flow-SPO | 0.76520 ^{†0.19355} | 0.85160 ^{†0.02121} |
| SuperFlow | 0.84128 ^{†0.26963} | 0.86851 ^{†0.03812} |

Table 2: Text Rendering and Human Preference Alignment results. OCR Score measures text rendering accuracy, while PickScore reflects human preference alignment. We highlight the **best**.

Text Rendering (OCR). As shown in Table 2, **SuperFlow** reaches 0.8413, improving over SD3.5-M (0.5717) by 47.2% and over Flow-GRPO (0.7252) by 16.0% at the same number of GPU Hours. Figure 2 shows that these gains hold across the five prompts, with **SuperFlow** achieving exact-match OCR in 4/5 cases. For the prompt “Fuel Low,” both SD3.5-M and Flow-GRPO score 0.00 due to missing or incorrect characters, while **SuperFlow** reaches 1.00 by reproducing the full string with the correct characters and spacing.

Human Preference Alignment (PickScore). As shown in Table 2, **SuperFlow** reaches 0.8685, a 4.6% gain over SD3.5-M (0.8304) and 1.7% over Flow-GRPO (0.8536) at the same number of training steps. For the prompt “a side view of a fox, with a flat design ...”, **SuperFlow** depicts far more details of the fox than SD3.5-M and Flow-GRPO.

7 Discussion and Ablation Study

7.1 Better Training Efficiency

Figure 1, 3, and 4 compare the training dynamics (reward versus training steps) of Flow-GRPO,

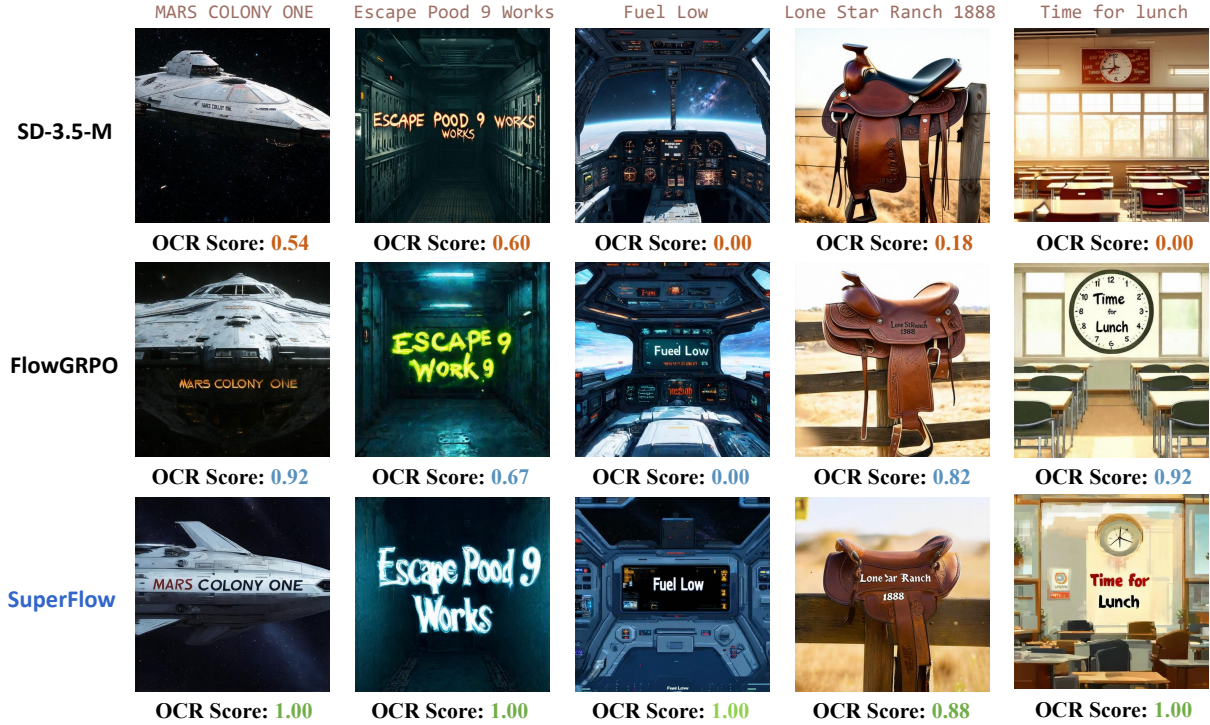


Figure 2: **SuperFlow**: Qualitative Comparison on the Visual Text Rendering Task. Our approach achieves higher text accuracy and readability compared with baselines.

| Model | Components | | Task Metrics | | |
|----------------------|--------------|--------------|-----------------------------------|-----------------------------------|-----------------------------------|
| | Adv-Est | Dyn-Samp | Geneval \uparrow | OCR Acc. \uparrow | PickScore \uparrow |
| Stable-Diffusion-3.5 | - | - | 0.57165 \uparrow 0.00000 | 0.57124 \uparrow 0.00000 | 0.83039 \uparrow 0.00000 |
| - | \checkmark | - | 0.79835 \uparrow 0.22670 | 0.82628 \uparrow 0.25504 | 0.86297 \uparrow 0.03258 |
| - | - | \checkmark | 0.79413 \uparrow 0.22248 | 0.70312 \uparrow 0.13188 | 0.86509 \uparrow 0.03470 |
| SuperFlow | \checkmark | \checkmark | 0.80451 \uparrow 0.23286 | 0.84128 \uparrow 0.27004 | 0.86618 \uparrow 0.03579 |

Table 3: Ablation Experiments on the Effectiveness of different components in **SuperFlow**. We highlight the best and second best results.

Flow-SPO, and **SuperFlow** across OCR, GenEval, and human preference alignment. Across both OCR and GenEval, **SuperFlow** exhibits consistently faster reward improvement and maintains a clear margin over Flow-GRPO throughout training. In the OCR task, for a fixed accuracy target in the 0.80–0.88 range, **SuperFlow** reaches the target using approximately 25–30% fewer GPU hours than Flow-GRPO. Similarly, on GenEval, **SuperFlow** learns more quickly and reaches 0.80 performance about 1.2 \times faster than Flow-GRPO. In human preference alignment, the reward of **SuperFlow** stays above or on par with the strongest baseline after the initial exploration phase, and attains 0.86 performance near 2 \times faster than FlowGRPO.

These trends directly reflect the effect of dynamic-group sampling. By allocating more samples to prompts with higher reward uncertainty

and reducing redundant sampling for low-variance prompts, **SuperFlow** concentrates computation on the most informative training signals. This targeted allocation accelerates reward improvement and shortens the time required to reach a given accuracy threshold without increasing total compute.

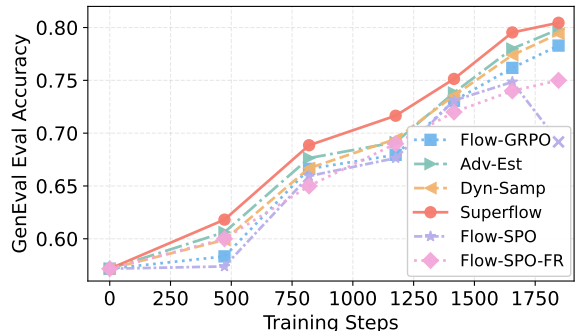


Figure 3: Training dynamics of different models on the compositional image generation task.

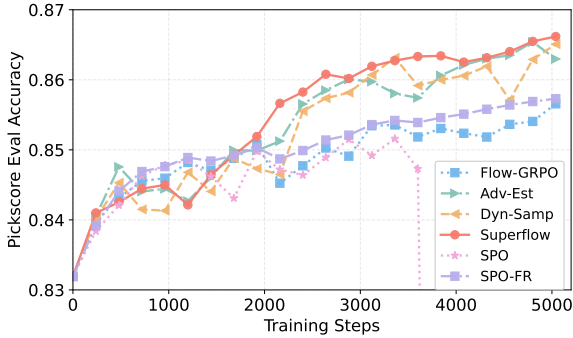


Figure 4: Training dynamics of different models on the human preference alignment task.

7.2 Improved Training Stability

In addition, Figure 1, 3, and 4 show that although Flow-SPO exhibits faster convergence and higher training efficiency than Flow-GRPO during the early and middle training phases, its training reward undergoes a sudden collapse in later stages. This behavior is consistently observed across all three datasets, indicating a pronounced instability in the training dynamics. The collapse suggests that single-rollout sampling, while efficient initially, fails to sustain reliable learning signals as policy entropy decreases and reward variance diminishes. In contrast, **SuperFlow** effectively mitigates this issue by replacing single-rollout sampling with dynamic group sampling. Throughout training, **SuperFlow** avoids reward collapse and maintains stable optimization trajectories. Moreover, it consistently exhibits lower step-to-step reward variance than all baselines, reflecting smoother learning dynamics and more reliable gradient estimates.

To verify that the Dynamic-Group Sampling strategy in **SuperFlow** effectively mitigates training collapse, Figure 4 shows that, while SPO collapses after step 3500, both Dyn-Samp and **SuperFlow** continue to improve beyond step 3500. This result clearly demonstrates that Dynamic-Group Sampling in **SuperFlow** enhances training stability without degrading overall training performance.

7.3 Effect of Proposed Components

Table 3 reports an ablation study on **SuperFlow** by isolating the effects of **Step-Level Advantage Re-estimation** (Adv-Est) and **Dynamic-Group Sampling** (Dyn-Samp). As shown, removing either part leads to a consistent performance drop. Removing either component results in consistent performance degradation. When only **Dynamic Sampling** is en-

abled, GenEval, OCR Accuracy, and PickScore decrease by 0.77%, 1.78%, and 0.37%, respectively, relative to the full model. In contrast, enabling only **Advantage Estimation** leads to a larger drop, particularly on OCR Accuracy, which decreases by 16.4%, along with a 1.29% reduction in GenEval. These results indicate that while both components individually contribute to performance gains across all metrics, their combination yields the greatest overall improvement.

7.4 Dynamic-Group Sampling VS Fixed Number of Group Rollouts

In this subsection, we evaluate the effectiveness of the proposed Dynamic-Group Sampling strategy by comparing **Dynamic-Group Sampling** (Dyn-Samp) against variants that use a fixed number of group rollouts (SPO-FR). In particular, we set the fixed group size to be 24, which matches the configuration used in Flow-GRPO (Liu et al., 2025) experiments and the maximum rollout count M_{max} used in Dyn-Samp.

We conduct experiments using the SD3.5-M (Esser et al., 2024b) as backbone and evaluate performance across three text-to-image tasks with different rewards. As shown in Figure 1,3, and 4, SPO-FR significantly improves training stability compared to single-rollout SPO, confirming the importance of multiple rollouts when directly applying SPO in flow-matching. Across three different text-to-image tasks, Dynamic-Group Sampling (Dyn-Samp) consistently outperforms SPO-FR in terms of final performance. By adaptively allocating rollouts based on prompt-level uncertainty, Dyn-Samp achieves stronger learning signals without incurring the uniform computational overhead associated with fixed group rollouts.

8 Conclusion

We presented **SuperFlow**, a method that integrates Single-Prompt Optimization into flow matching models. **SuperFlow** provides a practical framework for reinforcement learning in flow-based generative systems by combining dynamic sampling, adaptive value tracking, and variance-aware advantage re-estimation. The method improves training stability, reward efficiency, and generalization across diverse text-to-image tasks.

Limitations

Despite its effectiveness, the proposed method has several limitations. First, the dynamic-group sampling strategy uses reward uncertainty as a heuristic to estimate prompt informativeness, which may not fully capture all cases where additional exploration is beneficial. Finally, similar to other RL-based post-training approaches, the performance of our method remains dependent on the quality and stability of the reward signals, and noisy or imperfect rewards may limit the achievable gains. Extending the proposed framework to leverage richer or learned reward models, as well as applying it to other generative paradigms beyond flow matching, could be promising directions for future investigation.

Acknowledgment

This research is partially supported by a research award from Intuit AI Research and the award No. #2238940 from the Faculty Early Career Development Program (CAREER) of the National Science Foundation (NSF). The views and conclusions contained herein are those of the authors and should not be interpreted as necessarily representing the official policies, either expressed or implied, of the U.S. Government. The U.S. Government is authorized to reproduce and distribute reprints for governmental purposes notwithstanding any copyright annotation therein.

References

- James Betker, Gabriel Goh, Li Jing, Tim Brooks, Jianfeng Wang, Linjie Li, Long Ouyang, Juntang Zhuang, Joyce Lee, Yufei Guo, and 1 others. 2023. Improving image generation with better captions. *Computer Science*. <https://cdn.openai.com/papers/dall-e-3.pdf>, 2(3):8.
- Kevin Black, Michael Janner, Yilun Du, Ilya Kostrikov, and Sergey Levine. 2023. Training diffusion models with reinforcement learning. *arXiv preprint arXiv:2305.13301*.
- Jiuhai Chen, Zhiyang Xu, Xichen Pan, Yushi Hu, Can Qin, Tom Goldstein, Lifu Huang, Tianyi Zhou, Saining Xie, Silvio Savarese, Le Xue, Caiming Xiong, and Ran Xu. 2025a. Blip3-o: A family of fully open unified multimodal models-architecture, training and dataset. *CoRR*, abs/2505.09568.
- Jiuhai Chen, Le Xue, Zhiyang Xu, Xichen Pan, Shusheng Yang, Can Qin, An Yan, Honglu Zhou, Zeyuan Chen, Lifu Huang, Tianyi Zhou, Junnan Li, Silvio Savarese, Caiming Xiong, and Ran Xu. 2025b. Blip3o-next: Next frontier of native image generation. *CoRR*, abs/2510.15857.
- Renjie Chen, Wenfeng Lin, Yichen Zhang, Jiangchuan Wei, Boyuan Liu, Chao Feng, Jiao Ran, and Mingyu Guo. 2025c. Towards self-improvement of diffusion models via group preference optimization.
- Ganqu Cui, Yuchen Zhang, Jiacheng Chen, Lifan Yuan, Zhi Wang, Yuxin Zuo, Haozhan Li, Yuchen Fan, Huayu Chen, Weize Chen, Zhiyuan Liu, Hao Peng, Lei Bai, Wanli Ouyang, Yu Cheng, Bowen Zhou, and Ning Ding. 2025. The entropy mechanism of reinforcement learning for reasoning language models. *CoRR*, abs/2505.22617.
- Daya Guo DeepSeek-AI, Dejian Yang, Haowei Zhang, Junxiao Song, Ruoyu Zhang, Runxin Xu, and 1 others. 2025. Deepseek-r1: Incentivizing reasoning capability in llms via reinforcement learning.” *arxiv. Preprint posted online on*, 22:13–14.
- Zheng Ding and Weirui Ye. 2025. Treegrpo: Tree-advantage grpo for online rl post-training of diffusion models. *arXiv preprint arXiv:2512.08153*.
- Patrick Esser, Sumith Kulal, Andreas Blattmann, Rahim Entezari, Jonas Müller, Harry Saini, Yam Levi, Dominik Lorenz, Axel Sauer, Frederic Boesel, and 1 others. 2024a. Scaling rectified flow transformers for high-resolution image synthesis. In *Forty-first international conference on machine learning*.
- Patrick Esser and 1 others. 2024b. Scaling rectified flow transformers for high-resolution image synthesis. *arXiv preprint arXiv:2403.03206*.
- Lijie Fan, Tianhong Li, Siyang Qin, Yuanzhen Li, Chen Sun, Michael Rubinstein, Deqing Sun, Kaiming He, and Yonglong Tian. 2025. Fluid: Scaling autoregressive text-to-image generative models with continuous tokens. In *The Thirteenth International Conference on Learning Representations (ICLR)*.
- Ying Fan, Olivia Watkins, Yuqing Du, Hao Liu, Moonkyung Ryu, Craig Boutilier, Pieter Abbeel, Mohammad Ghavamzadeh, Kangwook Lee, and Kimin Lee. 2023. Dpok: Reinforcement learning for fine-tuning text-to-image diffusion models. *Advances in Neural Information Processing Systems*, 36:79858–79885.
- Dhruba Ghosh, Hannaneh Hajishirzi, and Ludwig Schmidt. 2023. Geneval: An object-focused framework for evaluating text-to-image alignment. *Advances in Neural Information Processing Systems*, 36:52132–52152.
- Lixue Gong, Xiaoxia Hou, Fanshi Li, Liang Li, Xiaochen Lian, Fei Liu, Liyang Liu, Wei Liu, Wei Lu, Yichun Shi, Shiqi Sun, Yu Tian, Zhi Tian, Peng Wang, Xun Wang, Ye Wang, Guofeng Wu, Jie Wu, Xin Xia, and 9 others. 2025. Seedream 2.0: A native chinese-english bilingual image generation foundation model. *CoRR*, abs/2503.07703.

- Xiaoxuan He, Siming Fu, Yuke Zhao, Wanli Li, Jian Yang, Dacheng Yin, Fengyun Rao, and Bo Zhang. 2025. Tempflow-grpo: When timing matters for grpo in flow models. *arXiv preprint arXiv:2508.04324*.
- Yuval Kirstain, Adam Polyak, Uriel Singer, Shahbuland Matiana, Joe Penna, and Omer Levy. 2023. Pick-a-pic: An open dataset of user preferences for text-to-image generation. *Advances in neural information processing systems*, 36:36652–36663.
- Black Forest Labs, Stephen Batifol, Andreas Blattmann, Frederic Boesel, Saksham Consul, Cyril Diagne, Tim Dockhorn, Jack English, Zion English, Patrick Esser, Sumith Kulal, Kyle Lacey, Yam Levi, Cheng Li, Dominik Lorenz, Jonas Müller, Dustin Podell, Robin Rombach, Harry Saini, and 2 others. 2025. Flux.1 kontext: Flow matching for in-context image generation and editing in latent space. *arXiv preprint arXiv:2506.15742*.
- Thanh-Long V Le, Myeongho Jeon, Kim Vu, Viet Lai, and Eunho Yang. 2025. No prompt left behind: Exploiting zero-variance prompts in llm reinforcement learning via entropy-guided advantage shaping. *arXiv preprint arXiv:2509.21880*.
- Junzhe Li, Yutao Cui, Tao Huang, Yinping Ma, Chun Fan, Miles Yang, and Zhao Zhong. 2025. Mixgrpo: Unlocking flow-based grpo efficiency with mixed ode-sde. *arXiv preprint arXiv:2507.21802*.
- Xinyao Liao, Wei Wei, Xiaoye Qu, and Yu Cheng. 2025. Step-level reward for free in rl-based t2i diffusion model fine-tuning. *arXiv preprint arXiv:2505.19196*.
- Yaron Lipman, Ricky TQ Chen, Heli Ben-Hamu, Maximilian Nickel, and Matt Le. 2022. Flow matching for generative modeling. *arXiv preprint arXiv:2210.02747*.
- Aixin Liu, Bei Feng, Bin Wang, Bingxuan Wang, Bo Liu, Chenggang Zhao, Chengqi Deng, Chong Ruan, Damai Dai, Daya Guo, and 1 others. 2024. Deepseek-v2: A strong, economical, and efficient mixture-of-experts language model. *arXiv preprint arXiv:2405.04434*.
- Jie Liu, Gongye Liu, Jiajun Liang, Yangguang Li, Jiaheng Liu, Xintao Wang, Pengfei Wan, Di Zhang, and Wanli Ouyang. 2025. Flow-grpo: Training flow matching models via online RL. In *Advances in Neural Information Processing Systems (NeurIPS)*.
- Xingchao Liu, Chengyue Gong, and qiang liu. 2023. Flow straight and fast: Learning to generate and transfer data with rectified flow. In *The Eleventh International Conference on Learning Representations*.
- Yifu Luo, Penghui Du, Bo Li, Sinan Du, Tiantian Zhang, Yongzhe Chang, Kai Wu, Kun Gai, and Xueqian Wang. 2025a. Sample by step, optimize by chunk: Chunk-level grpo for text-to-image generation. *arXiv preprint arXiv:2510.21583*.
- Yifu Luo, Xinhao Hu, Keyu Fan, Haoyuan Sun, Zeyu Chen, Bo Xia, Tiantian Zhang, Yongzhe Chang, and Xueqian Wang. 2025b. Reinforcement learning meets masked generative models: Mask-grpo for text-to-image generation. *arXiv preprint arXiv:2510.13418*.
- Yiyang Ma, Xingchao Liu, Xiaokang Chen, Wen Liu, Chengyue Wu, Zhiyu Wu, Zizheng Pan, Zhenda Xie, Haowei Zhang, Xingkai Yu, Liang Zhao, Yisong Wang, Jiaying Liu, and Chong Ruan. 2024. Janusflow: Harmonizing autoregression and rectified flow for unified multimodal understanding and generation. <https://arxiv.org/abs/2411.07975>.
- Dustin Podell, Zion English, Kyle Lacey, Andreas Blattmann, Tim Dockhorn, Jonas Müller, Joe Penna, and Robin Rombach. 2023a. SDXL: improving latent diffusion models for high-resolution image synthesis. *CoRR*, abs/2307.01952.
- Dustin Podell, Zion English, Kyle Lacey, Andreas Blattmann, Tim Dockhorn, Jonas Müller, Joe Penna, and Robin Rombach. 2023b. Sdxl: Improving latent diffusion models for high-resolution image synthesis. *arXiv preprint arXiv:2307.01952*.
- Michael Psenka, Alejandro Escontrela, Pieter Abbeel, and Yi Ma. 2023. Learning a diffusion model policy from rewards via q-score matching. *arXiv preprint arXiv:2312.11752*.
- Aditya Ramesh, Prafulla Dhariwal, Alex Nichol, Casey Chu, and Mark Chen. 2022. Hierarchical text-conditional image generation with clip latents. *arXiv preprint arXiv:2204.06125*, 1(2):3.
- Allen Z Ren, Justin Lidard, Lars L Ankile, Anthony Simeonov, Pulkit Agrawal, Anirudha Majumdar, Benjamin Burchfiel, Hongkai Dai, and Max Simchowitz. 2024. Diffusion policy optimization. *arXiv preprint arXiv:2409.00588*.
- Robin Rombach, Andreas Blattmann, Dominik Lorenz, Patrick Esser, and Björn Ommer. 2022. High-resolution image synthesis with latent diffusion models. In *Proceedings of the IEEE/CVF conference on computer vision and pattern recognition*, pages 10684–10695.
- Chitwan Saharia, William Chan, Saurabh Saxena, Lala Li, Jay Whang, Emily L. Denton, Seyed Kamyar Seyed Ghasemipour, Raphael Gontijo Lopes, Burcu Karagol Ayan, Tim Salimans, Jonathan Ho, David J. Fleet, and Mohammad Norouzi. 2022. Photorealistic text-to-image diffusion models with deep language understanding. In *Advances in Neural Information Processing Systems 35: Annual Conference on Neural Information Processing Systems 2022, NeurIPS 2022, New Orleans, LA, USA, November 28 - December 9, 2022*.
- John Schulman, Filip Wolski, Prafulla Dhariwal, Alec Radford, and Oleg Klimov. 2017. Proximal policy optimization algorithms. *arXiv preprint arXiv:1707.06347*.

Zhihong Shao, Peiyi Wang, Qihao Zhu, Runxin Xu, Junxiao Song, Xiao Bi, Haowei Zhang, Mingchuan Zhang, YK Li, Yang Wu, and 1 others. 2024. Deepseekmath: Pushing the limits of mathematical reasoning in open language models. *arXiv preprint arXiv:2402.03300*.

Richard S Sutton, David McAllester, Satinder Singh, and Yishay Mansour. 1999. Policy gradient methods for reinforcement learning with function approximation. *Advances in neural information processing systems*, 12.

Rui Tian, Mingfei Gao, Haiming Gang, Jiasen Lu, Zhe Gan, Yinfei Yang, Zuxuan Wu, and Afshin Dehghan. 2025. Unigen-1.5: Enhancing image generation and editing through reward unification in reinforcement learning. *arXiv preprint arXiv:2511.14760*.

Bram Wallace, Meihua Dang, Rafael Rafailov, Linqi Zhou, Aaron Lou, Senthil Purushwalkam, Stefano Ermon, Caiming Xiong, Shafiq Joty, and Nikhil Naik. 2024. Diffusion model alignment using direct preference optimization. In *Proceedings of the IEEE/CVF Conference on Computer Vision and Pattern Recognition*, pages 8228–8238.

Xinlong Wang, Xiaosong Zhang, Zhengxiong Luo, Quan Sun, Yufeng Cui, Jinsheng Wang, Fan Zhang, Yueze Wang, Zhen Li, Qiyang Yu, and 1 others. 2024. Emu3: Next-token prediction is all you need. *arXiv preprint arXiv:2409.18869*.

Jinheng Xie, Weijia Mao, Zechen Bai, David Junhao Zhang, Weihao Wang, Kevin Qinghong Lin, Yuchao Gu, Zhijie Chen, Zhenheng Yang, and Mike Zheng Shou. 2024. Show-o: One single transformer to unify multimodal understanding and generation. *arXiv preprint arXiv:2408.12528*.

Zhongwen Xu and Zihan Ding. 2025. Single-stream policy optimization. *CoRR*, abs/2509.13232.

Zeyue Xue, Jie Wu, Yu Gao, Fangyuan Kong, Lingting Zhu, Mengzhao Chen, Zhiheng Liu, Wei Liu, Qiushan Guo, Weilin Huang, and 1 others. 2025. Dancegrpo: Unleashing grpo on visual generation. *arXiv preprint arXiv:2505.07818*.

Renrui Zhang, Chengzhuo Tong, Zhizheng Zhao, Ziyu Guo, Haoquan Zhang, Manyuan Zhang, Jiaming Liu, Peng Gao, and Hongsheng Li. 2025a. Let’s verify and reinforce image generation step by step. In *Proceedings of the Computer Vision and Pattern Recognition Conference*, pages 28662–28672.

Tao Zhang, Cheng Da, Kun Ding, Huan Yang, Kun Jin, Yan Li, Tingting Gao, Di Zhang, Shiming Xiang, and Chunhong Pan. 2025b. Diffusion model as a noise-aware latent reward model for step-level preference optimization. *arXiv preprint arXiv:2502.01051*.

A GRPO on Flow Matching.

GRPO (Shao et al., 2024) employs a group-relative advantage. Given a prompt c , the flow model p_θ generates G samples $\{\mathbf{x}_0^i\}_{i=1}^G$ through reverse-time trajectories. The group-normalized advantage for trajectory i is defined as

$$\hat{A}_t^i = \frac{r(\mathbf{x}_0^i, c) - \text{mean}(\{r(\mathbf{x}_0^j, c)\}_{j=1}^G)}{\text{std}(\{r(\mathbf{x}_0^j, c)\}_{j=1}^G)}, \quad (15)$$

The policy is updated by maximizing

$$\mathcal{J}(\theta) = \mathbb{E}_{c \sim \mathcal{C}, \{\mathbf{x}^i\} \sim \pi_{\theta_{\text{old}}}(\cdot | c)} [f(r, \hat{A}, \theta, \varepsilon, \beta)], \quad (16)$$

where

$$f(r, \hat{A}, \theta, \varepsilon, \beta) = \frac{1}{G} \sum_{i=1}^G \frac{1}{T} \sum_{t=0}^{T-1} (A_t^i - \beta D_{\text{KL}}(\pi_\theta \| \pi_{\text{ref}})), \quad (17)$$

$$A_t^i = \min(r_k^i(\theta) \hat{A}_k^i, \text{clip}(r_t^i(\theta), 1 - \varepsilon, 1 + \varepsilon) \hat{A}_t^i) \quad (18)$$

$$r_t^i(\theta) = \frac{p_\theta(\mathbf{x}_{t-1}^i | \mathbf{x}_t^i, c)}{p_{\theta_{\text{old}}}(\mathbf{x}_{t-1}^i | \mathbf{x}_t^i, c)}, \quad (19)$$

B Single-Stream Policy optimization

Single-Stream Policy optimization (SPO) (Xu and Ding, 2025) introduces a framework that enables online policy updates using streaming rollouts by maintaining a per-prompt tracker to stabilize advantage normalization without sampling multiple rollouts.

Specifically, for each prompt c in the training set \mathcal{C} , SPO maintains a value tracker $\hat{v}(c)$ that stores the running estimate of the expected reward for prompt c . Specifically, $\hat{v}(c)$ is modeled using a Beta distribution $\hat{v}(c) \sim \text{Beta}(\alpha(c), \beta(c))$. The value tracker $\hat{v}_0(c)$ is first initialized using n_0 rollouts generated by the initial policy π_0 . For a specific prompt c , the value estimate is set to the empirical mean of the observed rewards $\{r_k\}_{k=1}^{n_0}$ obtained from these rollouts: $\hat{v}_0(c) = \frac{1}{n_0} \sum_{k=1}^{n_0} r_k$. The Beta parameters are then initialized using an equilibrium effective sample size N_0 :

$$\alpha_0(c) = N_0 \hat{v}_0(c), \quad \beta_0(c) = N_0 (1 - \hat{v}_0(c)). \quad (20)$$

The discount factor $\rho(c) = 2^{-D(c)/D_{\text{half}}}$ in Eq. 7 depends on the KL divergence $D(c)$ between the current policy and the last policy that acted on prompt c , so that larger policy shifts lead to faster forgetting. The hyperparameter D_{half} controls this forgetting rate $\rho \in [\rho_{\text{min}}, \rho_{\text{max}}]$.

C Details of the Experimental Setup

C.1 Implementation Details

We post-train all models on a single NVIDIA H200 GPU with 141 GB of memory. Unless stated otherwise, all methods use the same backbone model, prompt pool, reward computation, and training budget to ensure a controlled comparison. Unless specified otherwise, all hyperparameters follow the default values used in Liu et al. (2025) and all hyperparameters of SuperFlow are kept fixed across tasks except for the KL ratio β . or Dynamic-Group Sampling, we set the maximum rollout count M_{max} to be 24, matching the group size configuration used in Flow-GRPO and SPO-FR, and we set the number of uniform bins K to be 4 in all experiments. We use $T = 10$ discretization steps for flow-based sampling during RL training, and $T = 40$ steps for evaluation. The KL ratio β is set to 0.04 for GenEval and Text Rendering, and to 0.01 for PickScore. We adopt LoRA with the scaling factor $\alpha = 64$ and rank $r = 32$. Following Liu et al. (2025), for online variants we update the data collection policy every 40 RL training steps.

C.2 Dataset Specification

Visual Text Rendering. Text appears in many images, such as posters, book covers, and memes, so accurate and readable rendering is important for T2I models. Each prompt follows ‘‘A sign that says ‘text’’’, where ‘text’ is the exact string that should appear. We use 20K training prompts and 1K test prompts from Liu et al. (2025).

Following Gong et al. (2025), we define the reward as

$$r = \max(1 - N_e/N_{\text{ref}}, 0),$$

where N_e is the minimum edit distance between the rendered and target text, and N_{ref} is the number of characters inside the quotation marks in the prompt. In our implementation, the OCR system produces a single recognized string per image, and the edit distance is computed directly between the full OCR output and the target text, without sliding-window or substring matching. Prior to computing the edit distance, both strings are lowercased and stripped of punctuation and extra whitespace, following the protocol in Gong et al. (2025).

Compositional Image Generation.

GenEval (Ghosh et al., 2023) evaluates compositional prompts that involve counting, spatial

relations, and attribute binding across six sub-tasks. We use the official evaluation pipeline, which detects object boxes and colors and infers spatial relations. Training prompts are generated with the official scripts using templates and random combinations. We use the deduplicated test set from FlowGRPO (Liu et al., 2025) so that prompts that differ only by object order, such as “A and B” versus “B and A”, are treated as the same. We remove such variants from training. Based on the base model’s initial accuracy across the six tasks, we use the following prompt ratio during training: Position : Counting : Attribute Binding : Colors : Two Objects : Single Object = 7 : 5 : 3 : 1 : 1 : 0, following FlowGRPO (Liu et al., 2025). Rewards are rule-based. For **Counting**, we use $r = 1 - |N_{\text{gen}} - N_{\text{ref}}|/N_{\text{ref}}$. For **Position** and **Color**, the reward is defined hierarchically, conditioned on correct object count:

$$r_{\text{attr}} = \begin{cases} 0, & N_{\text{gen}} \neq N_{\text{ref}}, \\ \alpha, & N_{\text{gen}} = N_{\text{ref}} \wedge \neg C, \\ 1, & N_{\text{gen}} = N_{\text{ref}} \wedge C, \end{cases}$$

where C indicates whether the predicted spatial relation or color attribute is correct, and $\alpha \in (0, 1)$ denotes a partial reward assigned when the object count is correct but the attribute is incorrect.

Human Preference Alignment. We use PickScore (Kirstain et al., 2023) as the reward model. It is trained on human-annotated pairwise preferences for images generated from the same prompt. For each prompt–image pair, PickScore outputs a scalar reward that reflects prompt alignment and visual quality.

D Use of AI Assistants and Data Privacy

AI-assisted tools (e.g., ChatGPT and code completion systems) were used in a limited and supportive manner, primarily for improving code readability, debugging visualization scripts, and polishing English expression. All scientific decisions, experimental design, data processing, and interpretation of results were conducted and verified by the authors.

The datasets used in this work consist solely of publicly available benchmarks and model-generated data, and do not contain personally identifiable information or user-specific content. Therefore, no additional anonymization or privacy-preserving procedures were required.

Algorithm 1 SuperFlow training in Flow models

```

Set initial effective sample size  $N_0 = 1/(1 - \rho_{\min})$  # Initialize sample size

▷ Initializing
for each prompt  $c \in \mathcal{C}$  do
  Collect  $n_0$  rewards  $\{r_k\}^{n_0}$  with initial policy  $\pi_0$  # Collect initial rewards
  Compute initial value:  $\hat{v}_0(c) = \frac{1}{n_0} \sum_{k=1}^{n_0} r_k$  # Compute initial value
  Set  $\alpha_0(c) = N_0 \hat{v}_0(c)$ ,  $\beta_0(c) = N_0(1 - \hat{v}_0(c))$  # Set alpha and beta values
end for

▷ Training
for iteration  $i = 1, \dots, T$  do
  Compute sampling weights  $w_i(c)$  for all  $c \in \mathcal{C}$  (Eqn. 10). # Compute sampling weights
  Sample batch  $\mathcal{B}_i \subset \mathcal{C}$  of size  $B$  according to  $\{w_i(c)\}$ . # Sample batch
   $\mathcal{D} \leftarrow \emptyset$  # Initialize dataset

  ▷ Compute Raw Advantage
  for each  $c \in \mathcal{B}_i$  do
    Sample  $y \sim \pi_{\theta_{i-1}}(\cdot | c)$ , observe reward  $r(c, y)$ . # Sample action and observe reward
    Compute raw advantage  $A(c, y) = r(c, y) - \hat{v}_{i-1}(c)$ . # Compute raw advantage
  end for

  ▷ Policy Update
  Normalize:  $\tilde{A}(c, y) = \frac{A(c, y) - \mu_{\mathcal{B}_i}}{\sigma_{\mathcal{B}_i}} \times \eta \sigma_t$ . # Advantage Normalization
  Update tracker  $\hat{v}(c)$ ,  $\alpha(c)$ ,  $\beta(c)$  (Eq. 7). # Tracker Update
  Update policy  $\theta_{i-1} \rightarrow \theta_i$  with a policy gradient method. # Policy Update
end for

```

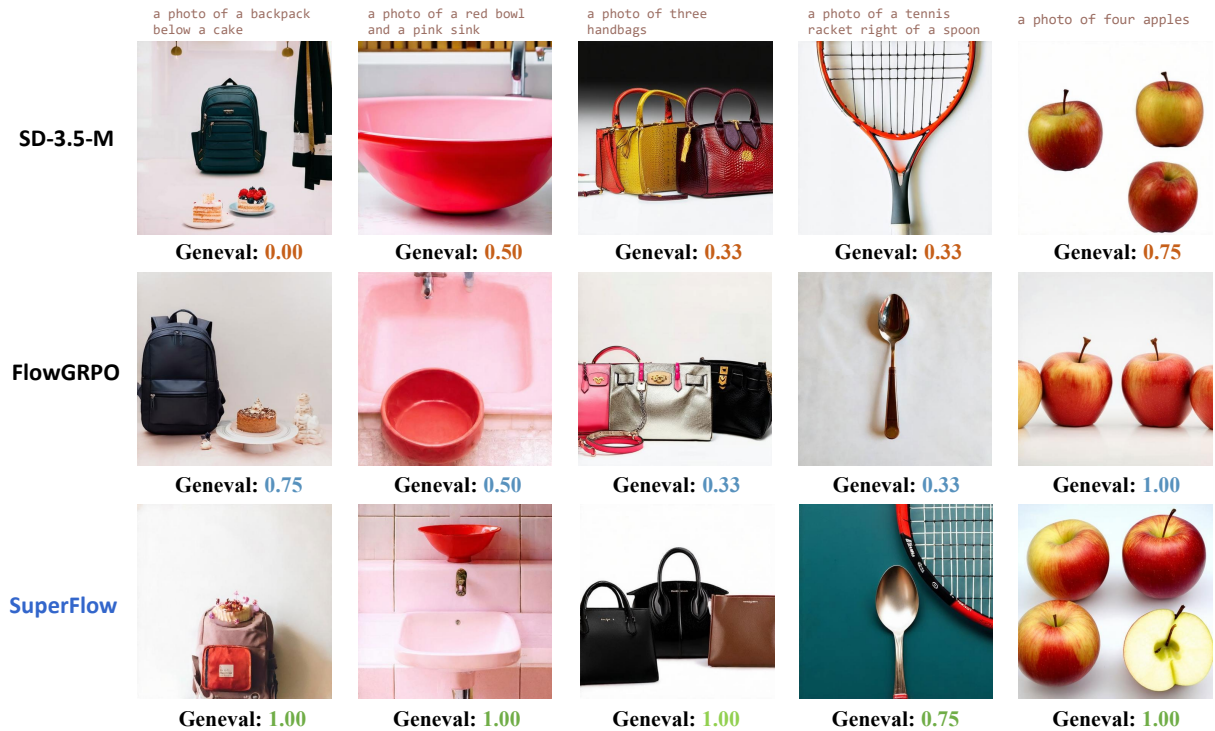


Figure 5: **SuperFlow: Qualitative Comparison on the Compositional Image Generation Task.** Our method improves accuracy in object composition, position, and attribute consistency.

| | a side view of a fox, with a flat design, artwork of t-shirt graphic. | a 300 x 300 px picture of a anime glowing orange rock | photo of traction engine in jungle river | anime portrait of eleven -e -w -1 in a post apocalyptic abandoned gas station with gas... | a man in a union jack outfit with cape, white lionhead emblem, photography... |
|------------------|--|--|--|---|--|
| SD-3.5-M |  PickScore: 0.88 |  PickScore: 0.82 |  PickScore: 0.84 |  PickScore: 0.78 |  PickScore: 0.82 |
| FlowGRPO |  PickScore: 0.90 |  PickScore: 0.83 |  PickScore: 0.87 |  PickScore: 0.79 |  PickScore: 0.86 |
| SuperFlow |  PickScore: 0.94 |  PickScore: 0.87 |  PickScore: 0.90 |  PickScore: 0.82 |  PickScore: 0.87 |

Figure 6: **SuperFlow: Qualitative Comparison on the Human Preference Alignment Task.** Our method produces images that better match human-preferred visual quality and prompt alignment.